Mon. Not. R. Astron. Soc. **340,** 52–58 (2003)

Statistics of turbulence profile at Cerro Tololo

A. Tokovinin,★ S. Baumont and J. Vasquez
Cerro Tololo Inter-American Observatory, Casilla 603, La Serena, Chile

Accepted 2002 October 29. Received 2002 October 28; in original form 2002 September 11

ABSTRACT

The results of a three-month continuous monitoring of the turbulence profile and seeing at Cerro Tololo (Chile) in 2002 May–July are presented. Some 28 000 low-resolution profiles were measured by a new MASS single-star turbulence monitor, accompanied by seeing data from DIMM. The median seeing was 0.95 arcsec. The first 500 m contribute 60 per cent to the total seeing, and the free-atmosphere median seeing was 0.55 arcsec. The free-atmosphere seeing is almost never better than 0.15 arcsec because there is always some turbulence above 12 km. A 4-d period of calm upper atmosphere with a stable free-atmosphere seeing of 0.2–0.3 arcsec was noted. The gain in resolution from adaptive compensation of the ground layer will be typically 1.7 times, and 2–3 times during such calm periods. Correlations of the free-atmosphere turbulence with the wind speed at the tropopause and of the ground-layer turbulence with the ground wind are studied. The temporal evolution of turbulence is characterized by recurrent bursts, their typical duration increasing from 15 min in low layers to 1–2 h in high layers. The large data base of turbulence profiles can be used to test mesoscale modelling of astronomical seeing.

Key words: turbulence – atmospheric effects – instrumentation: adaptive optics – site testing.

1 INTRODUCTION

A crucial role of 'seeing' in ground-based astronomy was recognized a long time ago. Nowadays it is possible to improve the seeing with adaptive optics (AO), but this technology is itself so dependent on the properties of turbulence that it has generated a new and important driver for detailed atmospheric studies. AO requires a knowledge of the temporal time constant and of the vertical turbulence profile, in addition to the overall (integrated) seeing. It is desirable to have reliable statistics of these parameters for a given site in order to predict the performance of AO systems. A real-time monitoring of optical turbulence would help in optimizing the AO operation. For example, the scintillometer of Ochs et al. was regularly operated at the AMOS station for this reason (Chonasky & Deuel 1988).

The vertical distribution of the optical turbulence strength (characterized by the altitude dependence of the refractive-index structure constant C_n^2) is notoriously difficult to monitor. Balloon-borne microthermal probes are expensive and sample the turbulence profile (TP) only once per flight, without any statistical averaging. Optical remote sounding by SCIDAR (Fuchs, Tallon & Vernin 1998) is free from this drawback, but it requires moderately large telescopes, sensitive detectors and powerful signal processing. For these reasons SCIDAR was only used in a campaign mode at existing observatories.

★E-mail: atokovinin@ctio.naoo.edu

A limited number of TPs measured world-wide revealed that turbulence is typically concentrated in a few thin layers. The physical mechanism generating such a distribution was studied by Coulman, Vernin & Fuchs (1995). It inspired designers of AO systems to add more deformable mirrors, each conjugated to its own layer, and thus to compensate seeing over a much wider field with such multiconjugate adaptive optics (MCAO) (Rigaut, Ellerbroek & Flicker 2000). The promising potential and wide popularity of MCAO added even more pressure to measure turbulence profiles; the Gemini site testing campaign at Cerro Pachón (Vernin et al. 2000; Avila et al. 2000) is an example of such an MCAO-driven study.

Next-generation ground-based telescopes with apertures of 20–100 m will include turbulence compensation already in their designs (Andersen, Ardeberg & Gilmozzi 2000). Sites for these telescopes are being selected with a strong weight given to AO-related turbulence parameters; site surveys based on seeing measurements alone, as was the case for the previous generation of telescopes, are no longer sufficient. Seeing is very much dominated by local and orographic effects that diminish the predictive power of seeing data. With modern computers, modelling of optical turbulence becomes feasible, giving new insights into the physics of seeing and new guidance to the choice of sites, e.g. Masciadri, Vernin & Bougeault (2001). However, computer models still need real TPs for their calibration.

A low-resolution turbulence profile monitor, the Multi-Aperture Scintillation Sensor (MASS), was developed in response to the needs of AO and MCAO, as well as the need for a portable instrument for site testing (Tokovinin & Kornilov 2002; Kornilov et al.

2002). MASS was operated in 2002 for several months at the Cerro Tololo Inter-American Observatory (CTIO) jointly with the Differential Image Motion Monitor (DIMM) (Boccas 2001). This paper presents the results of this campaign. It appears to be the most extensive data base of turbulence profiles existing to date world-wide.

Our aim was to gain some understanding of the turbulence localization above CTIO. We were specifically interested in the fraction of turbulence in the first few hundred metres above the ground and in the seeing that can be attained if these low layers were compensated by AO. *Ground-layer compensation* offers improved seeing in a much wider field than does classical AO (Rigaut 2002). This option is being studied for the 4.2-m SOAR telescope located close to CTIO on Cerro Pachón (Tokovinin et al. 2002), as well as for extremely large next-generation telescopes. Our work quantifies the gain expected from ground-layer compensation at a specific, good astronomical site, CTIO.

In Section 2 we briefly describe the instrumentation used in this study and give typical examples of the data. The statistics of the vertical turbulence distribution is explored in Section 3. Section 4 contains a summary and conclusions.

2 SITE, INSTRUMENTS AND DATA

2.1 Site

Cerro Tololo is located in Chile some 500 km to the north of Santiago (70° 48′ 52.″7 W, 30° 09′55.″ 5S). Altitude is 2200 m above sea level (a.s.l.). Among other Chilean sites, Cerro Tololo is known for its low ground wind speed.

The two instruments used in this campaign, the Multi-Aperture Scintillation Sensor (MASS) and the Differential Image Motion Monitor (DIMM), were placed at the northern edge of the summit, facing the direction of the prevailing wind (Fig. 1). DIMM is placed in a small tower some 6 m above the ground. The MASS feeding telescope was installed on the Losmandy equatorial mount, initially on the ground and later in a small dome.

2.2 MASS

MASS (Tokovinin & Kornilov 2002; Kornilov et al. 2002) measures low-resolution turbulence profiles from the scintillation of single stars. Light flux is received by four concentric-ring apertures with diameters of 2, 3.7, 7.0 and 13 cm and detected by photomultipliers in photon counting mode with 1 ms time sampling. Statistical analysis of the fluxes with 1 min accumulation time produces 10 scintillation indices that correspond to four individual apertures and six pair-wise aperture combinations. MASS is fed by a 14-cm off-axis reflecting telescope specially designed for this purpose.

At the beginning of a night, MASS is pointed to a bright ($V < 2^m$) blue single star close to zenith. After background measurement and star centring, a series of continuous 1-min integrations is started, with either manual or automatic guiding of the telescope. When zenith distance of the star increases above 45°, the telescope is repointed to another object (a total of three or four stars per night).

A model of turbulence distribution with six layers at fixed altitudes of 0.5, 1, 2, 4, 8 and 16 km above ground is fitted to the data. Each 'layer' represents in fact an integral of turbulence J_l,

$$J_l = \int_{\text{layer}} C_n^2(h) W(h)\, \mathrm{d}h, \qquad (1)$$

measured in $\mathrm{m}^{1/3}$, where $C_n^2(h)$ is the refractive-index structure constant in $\mathrm{m}^{-2/3}$ and $W(h)$ is the dimensionless response function of the instrument. MASS response functions are nearly triangular, going to zero at the altitudes of adjacent layers (Fig. 2). Thus, the 8-km layer measures, roughly, integrated turbulence strength from 6 to 12 km, while 16-km layer measures everything above 12 km. Turbulence at 6 km will show up in the 4-km and 8-km 'layers' with equal intensity. The sum of all response functions is constant (within 10 per cent) at altitudes above 0.5 km.

Atmospheric seeing ϵ_l (full width at half-maximum of a long-exposure image in a large telescope) produced by a turbulent layer can be computed from the intensity J_l. For ϵ_l in arcseconds at $\lambda =$ 500 nm and J_l in $\mathrm{m}^{1/3}$,

$$\epsilon_l = (J_l/6.8 \times 10^{13})^{3/5}. \qquad (2)$$

The sum of all layer intensities measured by MASS gives a good estimate of the 'free-atmosphere seeing' ϵ_f – the seeing that would be obtained without the contribution of turbulence in the first 500 m above ground. The free-atmosphere seeing is also estimated by MASS directly from a combination of three scintillation indices. There is a very good agreement between ϵ_f computed from the integrated profiles and directly. More details on the restoration procedure are given in Tokovinin et al. (in preparation). It is shown in this study that noise in MASS is signal-dependent, becoming smaller

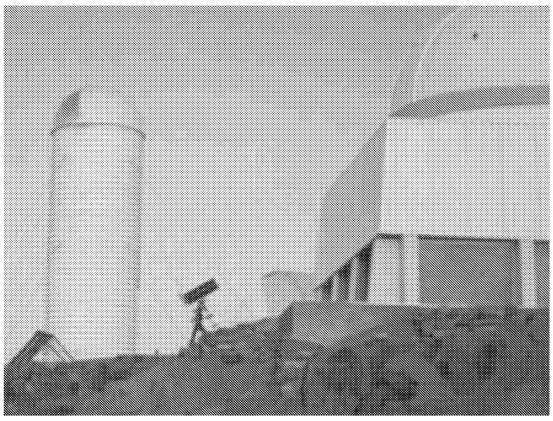

Figure 1. The DIMM instrument is installed in a 6 m high tower at the edge of Cerro Tololo summit. MASS was initially located on the ground, as shown; it was moved into the USNO dome (on the right) on 2002 May 19.

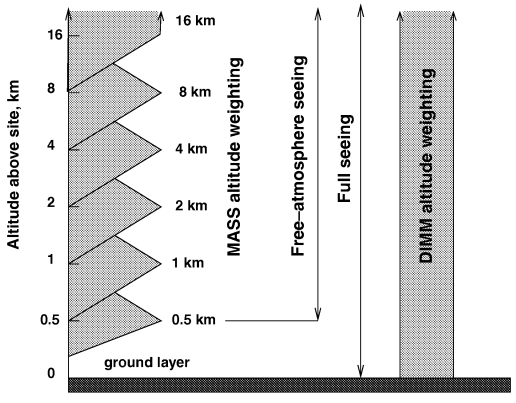

Figure 2. Scheme of the subdivision of atmospheric path into 0.5-km, 1-km, etc., layers measured by MASS and the total path measured by DIMM. Turbulence in the ground layer is inferred from the difference between DIMM and MASS.

under low-turbulence conditions. The strength of dominating layers is always measured with a typical relative error of 10 per cent which may be as low as 4×10^{-15} m$^{1/3}$ under calm conditions.

MASS data are reduced in real time and stored in an ASCII file, a profile every minute. Many additional parameters (instrumental configuration, stellar fluxes, quality of the model fit) are also written to this file. This permits any wrong data to be identified and rejected. The reasons for erroneous data are guiding errors, wrong background estimates and, by far most numerous, clouds. It was found that MASS gives consistent and reproducible results through thin cirrus clouds because slow light variations (below 1 Hz) are filtered out in the data reduction algorithm. We rejected only the data with low stellar fluxes and with flux variance (in 1 min with 1 s flux averaging) of more than 1 per cent that indicated varying cloud transmission during integration.

2.3 DIMM

DIMM measures the Fried parameter r_0 related to the full seeing $\epsilon = 0.98\,\lambda/r_0$ at wavelength λ (Sarazin & Roddier 1990; Tokovinin 2002). The seeing is deduced from the variance of the angle-of-arrival fluctuations (or image motion) is two small apertures.

The CTIO DIMM (Boccas 2001) uses the 25-cm Meade as feeding telescope. The diameter of the apertures is 95 mm (partially obstructed), and the distance between their centres is 15.3 cm. Images of a bright star formed by both apertures are separated by a wedge prism placed on one entrance aperture and detected by a charge-coupled device (CCD) camera with pixel size of 0.77 arcsec. Frame exposure time alternates between 5 and 10 ms, and the integration time for seeing estimate is 1 min, with acquisition rate about 300 images per minute. Upon background subtraction, the centroids of images are computed in a window of eight pixel radius. The variance of centroid coordinate differences in two orthogonal directions is corrected for noise variance and converted to seeing. The bias in seeing caused by finite exposure time is corrected by the modified exponential prescription as detailed in Tokovinin (2002). The DIMM data are stored in an ASCII file and are also available on the Internet in real time.

DIMM operates in a robotic mode, opening its dome and pointing at suitable stars when the meteorological conditions are adequate. Guiding is done between 1-min data accumulations. Robotic operation was interrupted repeatedly by failures to find a star, which called for manual interventions (the Meade mount does not have absolute position sensors to recover its pointing) and by failures of the drive motors, replaced several times. For this reason the time coverage of DIMM is somewhat less than that of MASS for the same period.

2.4 Comparison between MASS and DIMM

MASS and DIMM measure different 'seeings', ϵ_f and ϵ. Whenever the contribution of the first 500 m above ground to the total seeing is small, we must obtain $\epsilon_f \approx \epsilon$, otherwise the inequality $\epsilon_f < \epsilon$ must hold. This is indeed the case. In Fig. 3 we display a portion of data for the night of 2002 June 19–20 with very calm atmospheric conditions. Around 9.5 h UT an increased turbulence at 2 km dominated the seeing, with both instruments giving very similar results. For the rest of the night, the full seeing ϵ was very good, but still worse than ϵ_f because of ground-layer turbulence.

The condition $\epsilon_f \approx \epsilon$ illustrated above was not exceptional, but, on the contrary, was encountered regularly. Dominating high layers were frequently located at 0.5–1 km, but could be as high as 8 km. The agreement between the two very different instruments, MASS

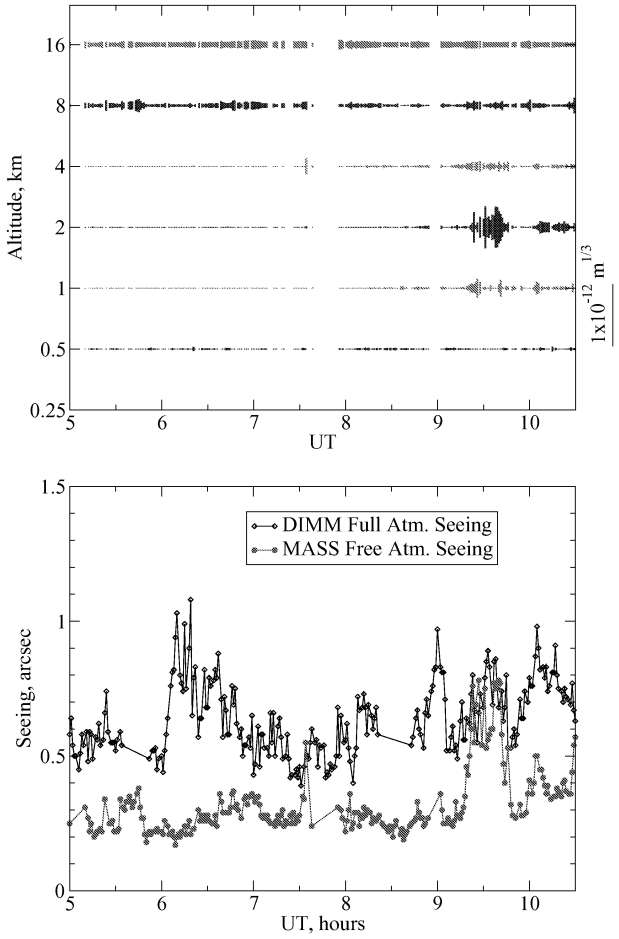

Figure 3. Turbulence profiles (top) and seeing (bottom) on the very calm night of 2002 June 19–20. Bars show the intensity of layers in m$^{1/3}$ with a scale indicated on the right.

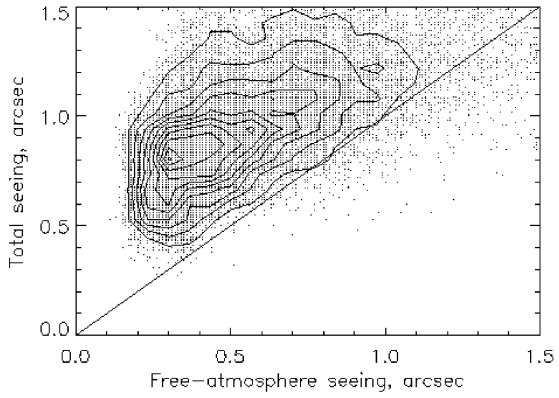

Figure 4. Comparison of the free-atmosphere seeing ϵ_f measured by MASS (horizontal axis) and the full seeing ϵ measured by DIMM (vertical axis) for all data in common. Contour plots are overlaid with 10 per cent intervals to show the density of points. The line shows $\epsilon_f = \epsilon$.

and DIMM, is better than one could expect; it gives confidence that both produce correct data.

Fig. 4 shows free-atmosphere seeing compared to the full seeing measured simultaneously (interpolated to the moments of MASS

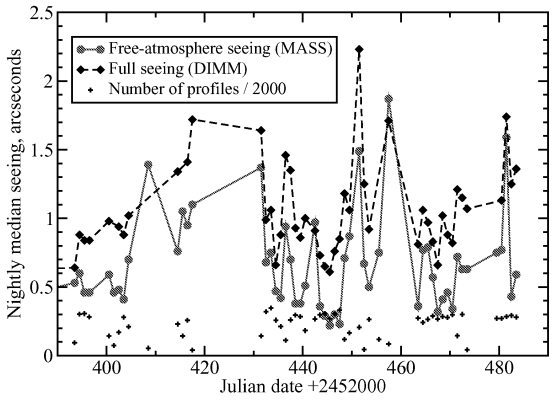

Figure 5. Nightly median values of total seeing ϵ and free-atmosphere seeing ϵ_f for the period 2002 April 29 to July 28. The crosses show the total number of TPs acquired each night (less than 500 on partially cloudy nights).

measurement from two adjacent DIMM points) for the whole data set. The occasional equality $\epsilon_f \approx \epsilon$ is clearly seen. A small number of points is located below the diagonal, $\epsilon_f > \epsilon$. These points can be explained by noise and by the fact that both instruments used different stars, so small localized patches of turbulence occasionally caused spikes in the MASS seeing not matched by DIMM. The inverse also happens, of course.

2.5 Data overview

The first useful MASS data were obtained on 2002 March 21–27 during the commissioning of this instrument. Systematic profile monitoring started on April 29. Here we consider the data obtained to July 28 inclusive, with three complete months covered. During this period MASS worked for 58 nights, but some of them were partially cloudy with a reduced number of data. On a clear night MASS measured some 500–600 profiles. The total number of TPs used for the analysis (after the cleaning mentioned above) is 22 300, of which 16 968 TPs have matching DIMM data.

The periods of bad weather are apparent in Fig. 5 where nightly median values of ϵ and ϵ_f are plotted. A particularly long cloudy period occurred between May 11 and June 6.

All seeing and TP data in this paper refer to the wavelength of 500 nm and to zenith. The following results characterize the atmosphere at Cerro Tololo in the period 2002 May–July. This corresponds to autumn and winter conditions, typically worse than average.

3 DATA ANALYSIS

3.1 Relative contribution of atmospheric layers to seeing

Table 1 contains the main levels of cumulative distributions of seeing: total ϵ, free-atmosphere ϵ_f and ground-layer seeing $\epsilon_g = (\epsilon^{5/3} - \epsilon_f^{5/3})^{3/5}$. In 7 per cent of cases with $\epsilon_f > \epsilon$ we assume that ground-layer seeing was close to zero. The data used for this analysis refer only to cases when both MASS and DIMM measurements are available. We also include the distribution of the isoplanatic angle θ_0, which is readily computed from MASS data.

Supposing that ground-layer turbulence can be measured and corrected by AO, we can estimate the resulting improvement in seeing. Of course, realistic adaptive optics will not correct ground-layer turbulence perfectly, but, on the other hand, it will partially correct higher layers. Still, the analysis presented in Table 2 and in Fig. 6 gives a quantitative idea of the gain in angular resolution expected from ground-layer correction. The gain increases when a thicker slab of turbulence is corrected, but at the same time the size of the corrected field becomes smaller.

Table 1 also contains the distribution of the fraction of C_n^2 integral contained in the first 500 m above the ground, $f_g = (\epsilon_g/\epsilon)^{5/3}$. We studied this parameter separately for good (<0.6 arcsec) and bad (>1 arcsec) seeing and did not find any substantial dependence. For example, median fractions of ground layer for good and bad seeing are 0.57 and 0.53, respectively. The largest median contribution of ground layer (0.66) is found for seeing between 0.6 and 1 arcsec. Turbulence profiles measured at the nearby mountain Cerro Pachón by Vernin et al. (2000) led to a model where the average contribution of ground layer is 65 per cent (Ellerbroek & Rigaut 2000).

Our results should be compared with the extensive monitoring of the turbulence profile at Cerro Tololo with generalized SCIDAR reported by Vernin et al. (2000) and Avila et al. (2000). These authors obtained 6900 TPs over 22 nights distributed in four campaigns throughout 1998. They find median total seeing of ϵ = 1.06 arcsec (0.85 arcsec when dome contribution is excluded), median free-atmosphere seeing $\epsilon_f = 0.56$ arcsec and median isoplanatic angle $\theta_0 = 2.14$ arcsec. The agreement with our data is encouraging. The free atmosphere was more perturbed in 1998 April and July compared to 1998 January and October. Thus, we expect that somewhat better seeing and larger isoplanatic angles will be measured during summer months.

Barletti et al. (1976) proposed a TP model based on 67 microthermal soundings. It predicts an average free-atmosphere seeing (all layers above 1 km) of 0.80 arcsec. Their 'lucky observer' model assumes the lowest turbulence levels measured at each altitude and predicts $\epsilon_f = 0.28$ arcsec. We see from Table 1 that such conditions are indeed encountered at Cerro Tololo 10 per cent of the time and that the median ϵ_f is significantly better than 0.80 arcsec. Marks (2002) used 15 soundings in Antarctica to claim that the upper atmosphere there is exceptionally calm, with a mean $\epsilon_f = 0.37$ arcsec. Equivalent or better conditions do occur at Cerro Tololo 25 per cent of the time even during the unfavourable winter months.

It is interesting that, even when all layers except the highest are corrected, the expected seeing is almost *never* better than 0.15 arcsec. The same conclusion is strikingly apparent in Fig. 4 where ϵ_f has a sharp lower cut-off at 0.15 arcsec. There is always

Table 1. Levels of the cumulative distributions of total seeing ϵ, free-atmosphere seeing ϵ_f, ground-layer seeing ϵ_g, fraction of ground layer and isoplanatic angle θ_0.

Probability	10 per cent	25 per cent	50 per cent	75 per cent	90 per cent
Total seeing, ϵ (arcsec)	0.64	0.79	0.95	1.17	1.43
Free-atm. seeing, ϵ_f (arcsec)	0.28	0.38	0.55	0.82	1.22
Ground-layer seeing, ϵ_g (arcsec)	0.24	0.47	0.66	0.83	1.02
Ground-layer fraction, f_g	0.11	0.38	0.60	0.76	0.85
Isoplanatic angle, θ_0 (arcsec)	2.94	2.36	1.80	1.30	0.98

Table 2. Levels of the cumulative distributions of seeing in arcseconds for different thicknesses of corrected layers.

Probability	10 per cent	25 per cent	50 per cent	75 per cent	90 per cent
No correction (ϵ)	0.64	0.78	0.95	1.17	1.46
Ground to 0.5 km (ϵ_f)	0.28	0.38	0.55	0.83	1.24
Ground to 2 km	0.22	0.30	0.43	0.62	0.92
Ground to 4 km	0.19	0.26	0.37	0.53	0.73
Ground to 8 km	0.15	0.20	0.29	0.43	0.60
Ground to 16 km	0.10	0.12	0.16	0.21	0.28

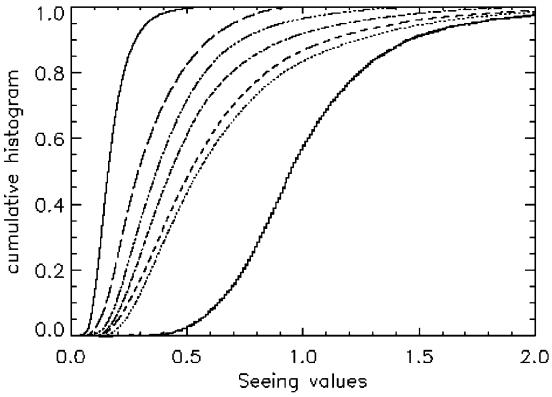

Figure 6. Cumulative distribution of the total seeing (thick line) and (from right to left) of the seeing that would result from correction of the ground layer, first 1 km, first 2 km, etc., to the seeing produced by the 16 km layer alone (leftmost curve).

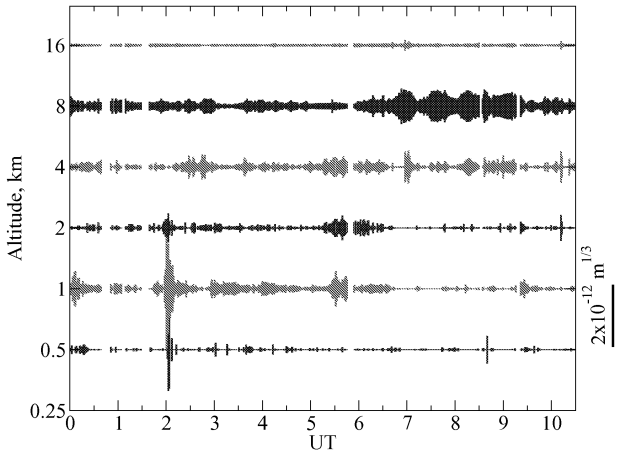

Figure 7. A typical night (2002 July 25–26) with turbulence bursts.

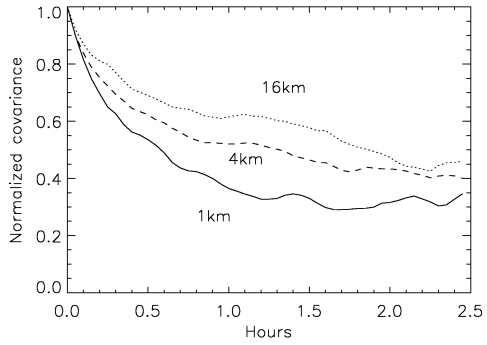

Figure 8. Normalized temporal autocorrelation functions of turbulence strength in three representative layers for the whole TP data base.

some non-negligible turbulence at the upper boundary of the troposphere (see also Fig. 9). Median C_n^2 integral in the 16 km layer is 3.2×10^{-14} m$^{1/3}$, some 10 times higher than the instrumental noise of MASS, which means that the effect is real and not related to some instrumental threshold. Vernin et al. (2000) measured the median seeing produced between 15 km and 20 km as 0.14 arcsec.

The consequences of this finding are important for adaptive optics. Even when the turbulence profile is completely dominated by a few strong and sharp layers, their correction by means of MCAO will not suffice to reach diffraction-limited resolution in a wide field because of the remaining high layers. The numbers in Table 2 indicate the median fraction of the 16 km layer as 5 per cent; a similar fraction of high-altitude turbulence is adopted in MCAO simulations for Gemini (Ellerbroek & Rigaut 2000). Another consequence of the upper-troposphere layers is the effective limit on isoplanatic field size θ_0: even under very calm conditions it practically never exceeds ~5 arcsec as measured at several sites. Median turbulence measured at the 16 km layer alone would give isoplanatic angle $\theta_0 = 13.4$ arcsec.

3.2 Temporal variation of turbulence

Strong bursts of turbulence that last typically for less than 0.5 h were observed repeatedly in almost all layers. An example of a typical night with perturbed atmosphere and bursts is given in Fig. 7 (note the coarser vertical scale compared to Fig. 3).

In Fig. 8 the normalized temporal autocorrelation functions $A(\Delta t)$ for low, intermediate and high layers are plotted. The data – layer intensities $J(t)$ – are not evenly spaced in time and have some gaps, making computation of covariance somewhat difficult. For this purpose we rebinned the $J(t_i)$ on a uniform grid with 3-min step, padding missing data with zeroes. The covariance $C(\Delta t)$ was then computed and transformed into autocorrelation $A(\Delta t)$:

$$C(\Delta t) = \frac{1}{N} \sum J(t_i) J(t_i + \Delta t), \tag{3}$$

$$A(\Delta t) = \frac{C(\Delta t) - \overline{J}^2}{C(0) - \overline{J}^2}, \tag{4}$$

where N is the total number of non-zero products for a time lag Δt and $\overline{J}$ is the average of J.

It can be seen that the time constant of turbulence variation is longer for high layers and shorter for low layers. At 50 per cent

correlation this time is 0.6, 1.3 and 1.9 h for 1, 4 and 16 km layers respectively. The autocorrelation functions show a fast decrease at small time lags that correspond to the presence of more rapid variations and are suggestive of power-law temporal spectrum. On the other hand, the 'tails' of $A(\Delta t)$ reflect long-term, night-to-night variations. If we subtract the tail from the 1 km autocorrelation, the 50 per cent correlation time would become 0.25 h, giving a better idea of the duration of turbulent bursts. Bursts are shorter than the periods between them, but $A(\Delta t)$ cannot reflect this difference.

Rich data on TPs enable a better understanding of the physics of atmospheric seeing. Seeing variations usually observed at good astronomical sites with a time-scale of ∼1.2 h (Sarazin 1997) can now be traced to the appearance turbulence bursts at specific altitudes. These bursts are a local phenomenon. We frequently compared the seeing at Cerro Tololo with the seeing at La Silla, only ∼100 km away: there is no correlation between seeing variations at these sites. Turbulence at medium altitudes must be related to the orographic disturbances. If at some lucky summit this turbulence could be avoided, it would enjoy a better and more stable seeing. Hydrodynamical modelling of turbulent flows is necessary to understand whether such 'lucky summits' indeed exist. On the other hand, it becomes evident that seeing statistics at any specific site is not necessarily representative of other mountains in the same region.

3.3 Seeing and weather

A period of calm atmosphere over Cerro Tololo shown in Fig. 3 actually lasted for four consecutive nights, from June 19 to 22. The free-atmosphere seeing was very stable at 0.2–0.25 arcsec; the burst shown in Fig. 3 is the worst $\epsilon_{\rm f}$ measured during this whole period. The total seeing as measured by DIMM was good but not exceptional. Seeing at the ESO sites La Silla and Paranal was also only moderately good. Based on DIMMs alone, one would never tell that something special was happening in the atmosphere on these dates. We have continuous profile data for the period from June 6 to June 30, with only small gaps due to cirrus clouds, which bracket this special period. Nightly median values of seeing, wind in the high atmosphere and at the ground for this period are listed in Table 3.

Investigation of meteorological conditions that produce extended periods of calm atmosphere is of evident practical interest if it can lead to understanding and prediction of such periods. A similar 3-d calm period was detected by R. Avila (private communication) in 2000 May at San Pedro Mártir in Mexico, with stable values of $\epsilon_{\rm f} \approx 0.2$ arcsec. This proves that calm atmosphere is something not very unusual. If all layers were independent of each other, the probability of all being quiet simultaneously would be low, and the probability of extended quiet periods would be vanishingly small. Instead, there must be a factor common to all layers that produces calm conditions in a systematic way, as noted for the first time by Barletti et al. (1976).

Table 3. Nightly median values of the full seeing ϵ, free-atmosphere seeing $\epsilon_{\rm f}$, wind speed at 200 mb, ground wind speed and direction for a calm period in 2002 June and adjacent dates.

Date, 2002	ϵ (arcsec)	$\epsilon_{\rm f}$ (arcsec)	$V_{200\,\rm mb}$ (m s^{-1})	$V_{\rm ground}$ (m s^{-1})
June 18	0.79	0.36	21.3	3.4 S
June 19	0.64	0.29	22.7	2.3 S
June 20	0.56	0.21	26.1	1.5 S
June 21	0.82	0.28	29.5	1.8 E
June 22	0.86	0.25	27.7	4.6 E
June 23	1.09	0.87	29.3	4.7 E

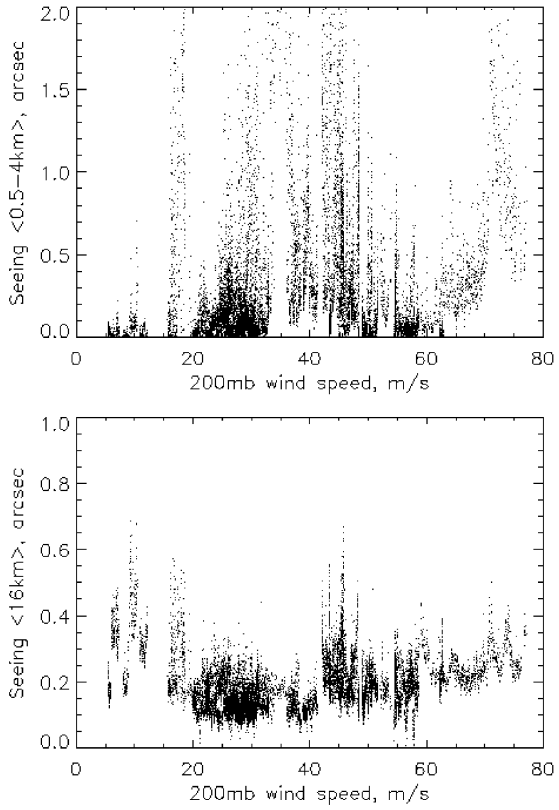

Figure 9. Correlation of the seeing generated by the low atmospheric layers (0.5–4 km, top) and by the 16-km layer (upper troposphere, bottom) with the wind speed at 200 mb level (12 km a.s.l.).

As a first attempt to understand quiet periods, we analysed the data on the speed of the jet stream (wind at 200 mb pressure or 12 km a.s.l.) over La Silla as collected by ESO. Indeed, the wind velocity $V_{200\,\rm mb}$ was low. We have data on $V_{200\,\rm mb}$ only up to 2002 July 4. Seeing produced by low and high layers is compared to $V_{200\,\rm mb}$ for this period in Fig. 9. The period studied is certainly not long enough to cover all representative meteorological conditions; the discussion that follows may be affected by a specific combination of weather patterns that occurred during this period.

Looking at Fig. 9, we note that there is no one-to-one correlation between jet stream and turbulence, but some tendencies do emerge. Low layers are generally more quiet when the jet stream speed is low. Of course, this may be related to the fact that wind speed and stability in all layers correlate with the 200 mb wind. The behaviour of the upper tropospheric layer (16 km), however, is noteworthy: it shows a clear minimum of turbulence for jet stream speeds between 20 and 40 m s^{-1}, whereas the turbulence increases for both faster and slower winds. Somehow a low jet stream is 'unnatural' for high atmosphere and causes more turbulence! Note that the high layer is never perfectly calm, unlike lower layers.

We also studied the relation between ground-layer seeing and ground wind as measured by the meteorological station on top of Cerro Tololo. Most frequently the ground wind blows from the north-east; otherwise it is from the south-west; the wind-rose clearly

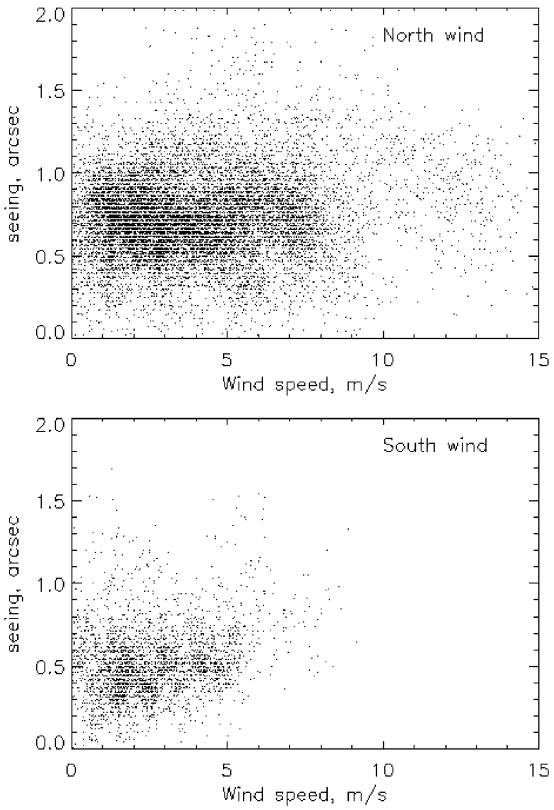

Figure 10. Correlation of the seeing ϵ_g generated by the ground layer (below 0.5 km) with the speed of the ground wind plotted separately for the north-eastern (top) and south-western (bottom) dominating wind directions.

shows these two dominating directions. We plot the ground-layer seeing ϵ_g against wind speed for these two directions separately in Fig. 10. There is practically no correlation for northern winds and some correlation for southern winds. Southern wind is definitely better for ground-layer seeing.

4 SUMMARY AND CONCLUSIONS

For a period of a few months we followed the evolution of optical turbulence over Cerro Tololo, for the first time being able to know where the 'seeing' comes from and why it changes. The data base of some 28 000 low-resolution TPs, most of which are complemented by seeing data, is unique in its volume and time coverage. The insights gained from these data can be summarized as follows:

(i) Ground-layer turbulence (first 500 m) at CTIO contributes 60 per cent of the total turbulence integral in 50 per cent of cases. Thus, a complete compensation of this layer would typically improve the seeing $0.4^{-3/5} = 1.7$ times.

(ii) The median free-atmosphere seeing ϵ_f (all layers above 500 m) is 0.55 arcsec, in 10 per cent of cases it is better than 0.28 arcsec, but it is practically never better than 0.15 arcsec. The effective lower limit to ϵ_f is related to the ever-present weak turbulence in the upper tropospheric layers above 12 km.

(iii) The periods of stably calm upper atmosphere with $\epsilon_f <$ 0.25 arcsec can be as long as a few days. This occurs when the wind velocity at 12 km a.s.l. is around 20–30 m s^{-1}. During these periods, the resolution gain from ground-layer AO compensation will be 2–3.

(iv) The characteristic time of turbulence variation increases with increasing layer altitudes, from 15 min (at 50 per cent correlation level) at 1 km to 1–2 h at 16 km. Often the turbulence at altitudes of 1–8 km has a character of recurrent strong bursts that last for ~0.5 h and repeat every 1–2 h.

Perhaps the most important impression from the data is the fragility of astronomical seeing. Most of the seeing results from local orographic effects and is significantly influenced by very unstable ground-layer turbulence. A common opinion that all good sites are similar and have a median seeing around 0.7 arcsec is in contradiction with the complexity of turbulence phenomena evidenced by this study. We believe that a better understanding and modelling of optical turbulence is possible and will help to choose 'lucky summits' that are much less affected by turbulence generated near surrounding mountains. Statistical data on TP will be essential for this work.

ACKNOWLEDGMENTS

This work makes extensive use of the data from CTIO DIMM developed by M. Boccas, N. Long, E. Bustos and H. E. M. Schwarz. The support of this campaign by the CTIO telescope operations staff was crucial and is acknowledged. Development of MASS and the observing campaign were supported by the 'Sites' programme of the New Initiatives Office of NOAO and managed by A. Walker.

REFERENCES

Andersen T., Ardeberg A., Gilmozzi R., eds, 2000, ESO Conf. Proc. 57, Proc. Backaskog Workshop on Extremely Large Telescopes, Backaskog, Sweden, 1999 June 1–2. ESO, Garching
Avila R., Vernin J., Chun M. R., Sánchez L., 2000, Proc. SPIE, 4007, 721
Barletti R., Ceppatelli G., Paternò L., Righini A., Speroni N., 1976, J. Opt. Soc. Am., 66, 1380
Boccas M., 2001, Description of CTIO DIMM, http://www. ctio.noao.edu/telescopes/dimm/dimm.html
Chonasky N., Deuel R. W., 1988, Appl. Opt., 27, 2214
Coulman C. E., Vernin J., Fuchs A., 1995, Appl. Opt., 34, 5461
Ellerbroek B. L., Rigaut F., 2000, Proc. SPIE, 4007, 1088
Fuchs A., Tallon M., Vernin J., 1998, PASP, 110, 86
Kornilov V., Tokovinin A., Vozyakova O., Zaitsev A., Shatsky N., Potanin S., Sarazin M., 2002, Proc. SPIE, 4839, paper 102
Marks R. D., 2002, A&A, 385, 328
Masciadri E., Vernin J., Bougeault P., 2001, A&A, 365, 699
Rigaut F., 2002, in Vernet E., Ragazzoni R., Esposito S., Hubin N., eds, Beyond Conventional Adaptive Optics, ESO Conf. Workshop Proc. No. 58. ESO, Garching, p. 11
Rigaut E., Ellerbroek B., Flicker R., 2000, Proc. SPIE, 4007, 1022
Sarazin M., 1997, Proc. SPIE, 3125, 366
Sarazin M., Roddier F., 1990, A&A, 227, 294
Tokovinin A., 2002, PASP, 114, 1156
Tokovinin A., Kornilov V., 2002, in Benkhaldoun Z., Muñoz-Tuñon C., Vernin J., eds, ASP Conf. Ser. Vol. 266, Astronomical Site Evaluation in the Visible and Radio Range, Marrakesh, 2000 November 13–17. Astron. Soc. Pac., San Francisco, p. 104
Tokovinin A., Gregory B., Schwarz H. E., Terebizh V., Thomas S., 2002, Proc. SPIE, 4839, paper 79
Vernin J. et al., 2000, Gemini Site Testing Campaign, Cerro Pachon and Cerro Tololo. Gemini RPT-AO-G0094, http://www. gemini.edu/

This paper has been typeset from a TEX/LATEX file prepared by the author.